Nuclear Instruments and Methods in Physics Research A 350 (1994) 327–337
North-Holland

NUCLEAR INSTRUMENTS & METHODS IN PHYSICS RESEARCH
Section A

Laboratory for Underground Nuclear Astrophysics (LUNA) ☆

U. Greife [a], C. Arpesella [b], C.A. Barnes [c], F. Bartolucci [b], E. Bellotti [d], C. Broggini [e], P. Corvisiero [f], G. Fiorentini [g], A. Fubini [h], G. Gervino [i], F. Gorris [a], C. Gustavino [b], M. Junker [a], R.W. Kavanagh [c], A. Lanza [f], G. Mezzorani [j], P. Prati [f], P. Quarati [k], W.S. Rodney [l], C. Rolfs [a,*], W.H. Schulte [a], H.P. Trautvetter [a], D. Zahnow [a]

[a] *Institut für Physik mit Ionenstrahlen, Ruhr-Universität Bochum, Germany*
[b] *Laboratori Nazionali del Gran Sasso, LNGS, Assergi, Italy*
[c] *Kellogg Radiation Laboratory, Caltech, Pasadena, USA*
[d] *Dipartimento di Fisica and INFN, Milano, Italy*
[e] *INFN, Padova, Italy*
[f] *Dipartimento di Fisica and INFN, Genova, Italy*
[g] *Dipartimento di Fisica and INFN, Ferrara, Italy*
[h] *ENEA, Frascati and INFN, Torino, Italy*
[i] *Dipartimento di Fisica Sperimentale and INFN, Torino, Italy*
[j] *Dipartimento di Scienze Fisiche and INFN, Cagliari, Italy*
[k] *Politecnico, Torino and INFN, Cagliari, Italy*
[l] *Georgetown University, Washington, USA*

Received 8 June 1994

A compact high-current 50 kV ion accelerator facility including a windowless gas target system, a beam calorimeter, and detector telescopes in close geometry has been built and tested. The data acquisition and analysis involved a multiparameter system and a Monte Carlo program. The LUNA facility, presently installed at the Gran Sasso underground laboratory, is a pilot project focused initially on cross section measurements of the ^{3}He(^{3}He, 2p)^{4}He reaction within the thermal energy region of the sun. To achieve this goal, the experimental sensitivity has been improved by more than four orders of magnitude over that of previous work.

1. Introduction

Thermonuclear reactions are important in understanding the generation of energy and the synthesis of elements in stars [1,2]. Due to the Coulomb barrier of the entrance channel, the reaction cross section $\sigma(E)$ drops nearly exponentially with decreasing energy E (E = center-of-mass energy), thus it becomes increasingly difficult to measure $\sigma(E)$. Indeed, it was not yet possible to measure $\sigma(E)$ within the thermal energy region in stars. Instead, the observed energy dependence of $\sigma(E)$ at higher energies had to be extrapolated to thermal energies. The extrapolation is facilitated if the cross section data are transformed into the astrophysical $S(E)$ factor defined by the equation $\sigma(E) = S(E)E^{-1}\exp(-2\pi\eta)$, where η is the Sommerfeld parameter. Of course, the larger the energy gap between the lowest experimental energy point and thermal energies, the higher the uncertainty in the extrapolated $\sigma(E)$, or equivalently $S(E)$. Although experimental techniques have been improved over the years to extend measurements to lower energies, this goal was severely hampered by the effects of cosmic rays in the detectors.

It is well known that two different sets of reactions can convert hydrogen into helium in sufficient amounts to provide the energy needed for a star's luminosity: the p–p chain and the CNO cycles. Both mechanisms have the same basic scenario, in which a series of two-body interactions and beta-decays produce the same result: $4p \rightarrow {}^4He + 2e^+ + 2\nu$ (+27 MeV). By the end of the 1950s, initial laboratory measurements as well as theoretical work had been performed on the cross sections and decay rates of each of the important nuclear processes in the p–p chain and the CNO cycles, and then extrapolated and corrected for conditions in the stellar interior (e.g. in the sun, with a central temperature of 15×10^6 K). In the standard solar model [3] it was calculated that 98.5% of the energy in the sun comes from the p–p chain reactions and 1.5% from the reactions in the CNO cycles. In the 1950s the possibility

☆ Supported in part by the Bundesminister für Forschung und Technologie (FKZ: 06B0631), DAAD-Vigoni (italian and german supports), and INFN.

* Corresponding author. Tel. +49 234 700 3602, fax +49 234 709 4172, e-mail rolfs@ep3.ruhr-uni-bochum.de.

SSDI 0168-9002(94)00703-A

and significance of detecting some of the neutrinos produced in the solar hydrogen-burning processes was recognized [4]. This led to the development of the ^{37}Cl solar neutrino detector, with a threshold at 0.8 MeV, named HOMESTAKE. In recent years, another technique was developed utilizing ^{71}Ga with a threshold at 0.2 MeV, named GALLEX and SAGE. Finally, the KAMIOKANDE II detector has been in operation for several years, with a threshold at 7 MeV. All these solar neutrino detectors have observed a neutrino flux from the sun. The GALLEX and SAGE detectors observed for the first time the high flux of the low-energy pp-neutrinos, in an amount of about two-thirds of the expected flux, while the observed flux of the high-energy neutrinos in KAMIOKANDE and HOMESTAKE is about a factor 2 and 3 lower than expected, respectively. However, these observations of different parts of the solar neutrino spectrum [3] presently provide no unique picture. Possible solutions could be found in the fields of neutrino physics, solar physics, or nuclear physics. The present status of knowledge of the cross sections and decay rates of the important nuclear processes in the p–p chain and CNO cycles has been reported recently [5]. We discuss here only two more relevant nuclear aspects: the case of the ^{3}He(^{3}He, 2p)^{4}He reaction (p–p chain) and the effects of electron screening.

Studies of the ^{3}He(^{3}He, 2p)^{4}He reaction have been carried out [6–8] over a wide range of energies, down to $E = 90$ keV. The $S(E)$ factor data are nearly energy-independent and have been fitted to a polynomial function with $S(0) = 5.5$ MeV b. Based partially on theoretical arguments, it was suggested [9,10] that a low-energy resonance might exist in this reaction. Such a resonance would correspond to an excited state in ^{6}Be near the ^{3}He + ^{3}He threshold. However, searches for this state, using a variety of other nuclear reactions, have not been successful [11]. Dwarakanath [12] carried out a direct search for this hypothetical resonance state by extending the ^{3}He-(^{3}He, 2p)^{4}He reaction studies down to $E = 30$ keV. Although the data might allow an increase in the $S(E)$ factor at the lowest energies, the 200% uncertainties in the data points below 40 keV precluded any rigorous conclusions. Another direct search was carried out by Krauss et al. [13] to energies as low as $E = 25$ keV ($\sigma = 7 \pm 2$ pb). The data give no evidence for a resonance. Thus, the hypothetical resonance can only be located below 25 keV.

In the extrapolation of $\sigma(E)$ the following assumption is made: the Coulomb potential of the target nucleus and projectile is that resulting from bare nuclei. However, for nuclear reactions studied in the laboratory, the target nuclei and projectiles are usually in the form of neutral atoms/molecules and ions, respectively. The electron clouds surrounding the interacting nuclides act as a screening potential [14]: the projectile effectively sees a reduced Coulomb barrier. This in turn leads to a higher cross section, $\sigma_s(E)$, than would be the case for bare nuclei, $\sigma_b(E)$. There is, in fact, an enhancement factor $f(E) = \sigma_s(E)/\sigma_b(E) \simeq \exp(\pi\eta U_e/E)$, where U_e is the electron screening potetial. Note that $f(E)$ increases exponentially with decreasing energy E. For energy ratios $E/U_e \geq 1000$, shielding effects are negligible, and laboratory experiments can be regarded as essentially measuring $\sigma_b(E)$. However, for $E/U_e \leq 100$, shielding effects become important for understanding and extrapolating low-energy data. Recent low-energy studies of ^{3}He(d, p)^{4}He showed [15] for the first time the screening effects. Subsequent studies of other fusion reactions also showed the expected exponential enhancement of the cross section at low energies (Ref. [16] and references therein). However, the observed enhancement was in all cases significantly larger than could be accounted for from available atomic physics models. An exception to the above observations occurs in the data of ^{3}He(^{3}He, 2p)^{4}He, which show a relatively flat $S(E)$ curve down to 25 keV, although the effects of electron screening should have enhanced the data at 25 keV by at least a factor 1.2. Thus, improved low-energy data are highly desirable for this and other fusion reactions.

As noted above, the low-energy studies of thermonuclear reactions in a laboratory at the earth surface are hampered predominantly by the effects of cosmic rays in the detectors. Passive shielding around the detectors provides a reduction of gammas and neutrons from the environment, but it produces at the same time an increase of gammas and neutrons due to the cosmic ray interactions in the shielding itself. A 4π active shielding, which is difficult to implement and also expensive, can only partially reduce the problem of cosmic ray activation. The best solution is to install an accelerator facility in a laboratory deep underground, such as in the Laboratori Nazionali del Gran Sasso [17] (LNGS), where the flux of cosmic ray muons is reduced [18] by a factor of 10^6. We report here on such a "Laboratory for Underground Nuclear Astrophysics" (called LUNA) installed at LNGS, which respresents a pilot project centered around a 50 kV accelerator. The LUNA project is initially focused on renewed studies of the ^{3}He(^{3}He, 2p)^{4}He reaction (including electron screening effects) covering nearly the entire thermal energy region in the sun ($E_0 = 16$ to 27 keV for $T = 15.5 \times 10^6$ K). To achieve this goal, the sensitivity of the experiment had to be improved by several orders of magnitude compared to Ref. [13]. We report here on the technical problems and their solutions. Additional details of this work can be found in Refs. [19–21].

2. Experimental equipment and setup

Previous investigations of the ^{3}He(^{3}He, 2p)^{4}He reaction [13] used a 100 kV accelerator at the Dynamitron Tandem Laboratorium (DTL) in Bochum in combination with a windowless gas target system with tight pumping apertures (smallest diameter: 4 mm) in front of the target area. At an energy of 100 keV the accelerator provided ion currents in

the target area of several 100 μA. However, at lower energies the current dropped continuously, such that at 10 keV only a few μA were available. This current reduction is predominantly due to the known effects of space charge repulsion within the ion beam and is visible in particular at low ion energies and high ion currents. In order to minimize such space charge effects [22,23], the path length of the ion beam between the ion source and the target area should be as short as possible (100 kV accelerator: about 7 m; aim of the 50 kV LUNA accelerator: less than 1 m, i.e. a compact design), and the beam transport system should contain only magnetic elements (in order to minimize the extraction of secondary electrons accompanying the ion beam, which themselves compensate in part the ion beam charges). Furthermore, since the cross section drops steeply at energies far below the Coulomb barrier, a precise knowledge of the absolute projectile energy (aim: $\Delta E/E \leq 1 \times 10^{-4}$), its long term stability, and the projectile energy spread (aim: ≤ 25 eV) is needed. In addition to these specifications, the 50 kV LUNA accelerator should provide currents of hydrogen and helium ions of order of several 100 μA in the target area at energies 10–50 keV. It should also allow a connection in situ to accelerators of higher energy (for tests and calibrations) and it should be built as a movable facility.

The basic concept of the accelerator consisted of a high-current ion source, an ion beam extraction and acceleration system, a double-focusing analysing magnet, and a beam-defining aperture near the target area. Beam transport calculations (in first order) indicated that with a 90° magnet placed at a distance of 0.35 m from the ion source the ion beam can be focused to a spot of less than 4 mm diameter at a target distance of 0.85 m from the ion source. The actual design of the various components of this accelerator facility (Fig. 1) are described in the following subsections. The 50 kV LUNA accelerator facility was designed, built, and tested at the Ruhr-Universität Bochum and was moved to LNGS.

2.1. Ion source

Two duoplasmatron ion sources were available: model PSX-100 from Peabody Scientific and a home-made source constructed similar to the Ortec model 350. Both ion sources have a tungsten outlet of 0.25 mm diameter (anode) and deliver a few mA total beam current for hydrogen and helium ions. The energy spread of such ion sources is less than 20 eV and the plasma potential deviates by less than 10 V from the voltage applied to the anode [24]. The sources provide a stable ion beam current over periods of

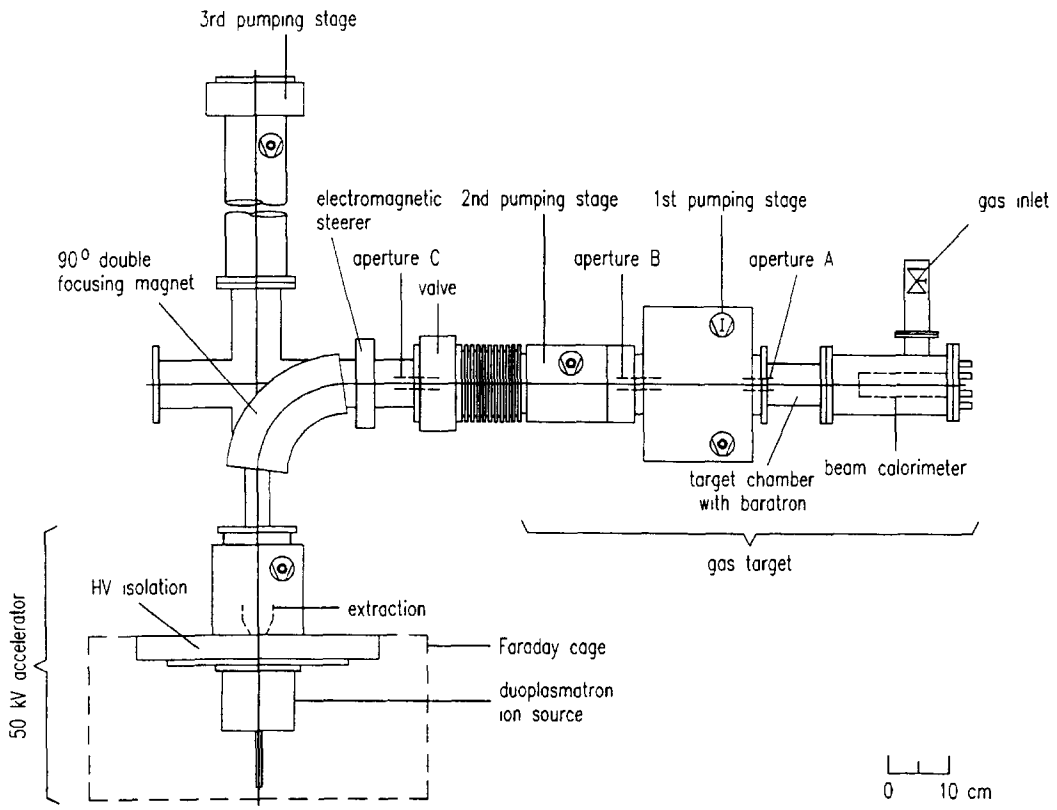

Fig. 1. Schematic diagram of the 50 kV LUNA accelerator facility.

up to 4 weeks. The gas flow into the ion source is regulated by a piezo valve (model PV10, Veeco) in combination with a thermocouple gauge. The cooling of the ion source is provided by a Freon R113 circuit (closed system).

The home-made DC power supplies for the ion source magnet (max. 3 A, 200 V), the filament (max. 35 A, 5 V), and the arc discharge (400 V ignition; 3 A, 110 V operation) are mounted on an electrically insulated high voltage (HV) platform and are surrounded by a Faraday cage. In order to keep the possible damage caused by HV sparks as small as possible, the power supplies are not regulated electronically. Instead, the parameters of the power supplies are chosen with adjustable transformers. The AC fraction of the output of the power supplies is smoothed to mV amplitudes using LC elements, thus minimizing intensity modulations of the ion beam current. The electric power on the HV platform is provided by 3 HV separation transformers (70 kV insulation, type BV21273, Schuhmacher) capable of transforming 7.5 kW. The necessary power for the ion source system is led via a shielded cable tunnel to the ion source area; the cable tunnel consists of polyethylene surrounded by a metal tube. For safety, the complete system is controlled by an interlock alarm system.

2.2. High voltage

The high voltage of the accelerator is provided by a HCN 1300–65000 power supply (FUG), with specifications such as max. 65 kV/20 mA, reproducibility $= 1 \times 10^{-3}$, ripple $< 1 \times 10^{-4}$ (typical: 5×10^{-5}), stability (8 h) $< 1 \times 10^{-4}$, and temperature coefficient $< 1.5 \times 10^{-4}$/K. In order to know the HV with the desired precision of 1×10^{-4} as well as to monitor the HV under varying conditions of room temperature and humidity (minimized in the air conditioned laboratory room at LNGS, with a temperature of $T = 20$°C and a relative humidity of $H = 35\%$, Section 2.10), an external HV determination was needed. The device used consists of a resistor chain, contained in an air-tight Plexiglas tube, and a digital multimeter. The resistor chain is built as a voltage divider with fifty 20 MΩ and one 100 kΩ high precision resistors, where the resistors have a temperature coefficient of 1×10^{-5}/K and can sustain each a voltage of up to 12 kV (resistor type 968.3, Metallux). The high number of resistors was used to keep the HV difference on each resistor small and thus to minimize the possibility of surface effects. The digital multimeter (model HP 34401A, Hewlett-Packard) has a long term stability of 5×10^{-5} per year and provides the voltage U_m measured across the 100

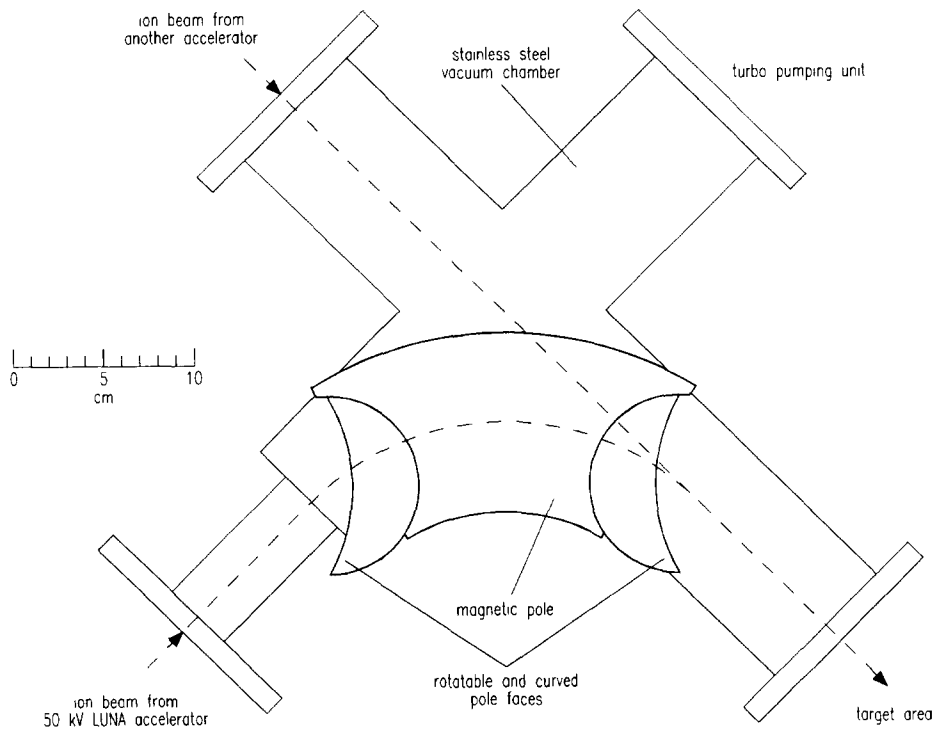

Fig. 2. Diagram of the double focusing 90° bending magnet with variable entrance and exit pole faces. The magnet chamber has ports for the ion beam path from the 50 kV accelerator, a turbo pump, and a connection to other accelerators (for tests and calibrations).

kV resistor. The HV device was calibrated at the Physikalisch–Technische Bundesanstalt in Braunschweig (Germany) – at $T = 20 \pm 1$°C and $H = 35 \pm 10\%$ – to a precision of 5×10^{-5} in the region of $U_{true} = 5$ to 80 kV, leading to $U_{true} = U_m$ $(10107.3 - 0.044U_m + 3.5 \times 10^{-4}U_m^2)$, with U_{true} and U_m in kV.

2.3. Movable extractor

The compact design of the accelerator facility required that the extraction voltage is identical to the acceleration voltage. Thus, at lower ion beam energies (acceleration voltages) the electric fields are lower, which in turn leads to a lower beam current extracted from the ion source. To minimize this effect, the extraction system was constructed as a unit allowing one to move in situ the electrode closer to the ion source, thus maintaining a high electric field at all ion beam energies. It was found that the ion beam current can be increased e.g. at 5 keV by at least a factor 3 compared to that with the extractor placed at the 50 keV position. Tests using an accel–decel–extraction system led in this setup only to a further ion current improvement of about 10%, but raised cooling problems in the extraction system; this alternative solution was thus not followed further.

2.4. Double focusing 90° bending magnet

In the compact design of the LUNA accelerator the 90° bending magnet had not only to analyse the ion beam species from the ion source but also to focus them on the target. The requirement of double focusing of a sector magnet can be achieved with inclined entry and exit faces of the magnet. For a proper choice of the angles of the entry and exit faces astigmatic focusing can be achieved, where the proper values of these angles depend on the design of the ion beam system, but generally they lie in the range between 25° and 40°. To find empirically the proper angles in the present setup, the home-made 90° bending magnet (bending radius: 15 cm) was designed with rotatable entrance and exit pole faces (Fig. 2). The optimum angle for both sides turned out to be at 40°. The magnet was made of special steel (AME1S, Saarstahl) with a low concentration of carbon and other elements leading to a low coercive field. Perturbations of second order in the magnetic field, or asymmetries in the incident ion beam profile, can be compensated with a sextupole field. Such a sextupole field can be produced by carving a curvature into the inclined pole faces: it was found empirically that a curvature of 30 cm radius was sufficient to compensate for second order imaging effects. Finally, to adjust the ion beam path after the magnet properly to the beam axis, a magnetic steerer for vertical corrections was installed after the magnet (Fig. 1).

2.5. Beam transmission on target

With a solid target setup and a beam limiting aperture of 20 mm diameter near the target, the accelerator provided analysed hydrogen and helium ion beam currents of about 1 mA on target in the energy range 30 to 50 keV, which represents nearly a 100% transmission. Below 30 keV the transmission dropped to values of 87, 71, 47, 24, and 7% at energies 25, 20, 15, 10, and 5 keV, respectively. Thus, at energies as low as 10 keV a beam current of about

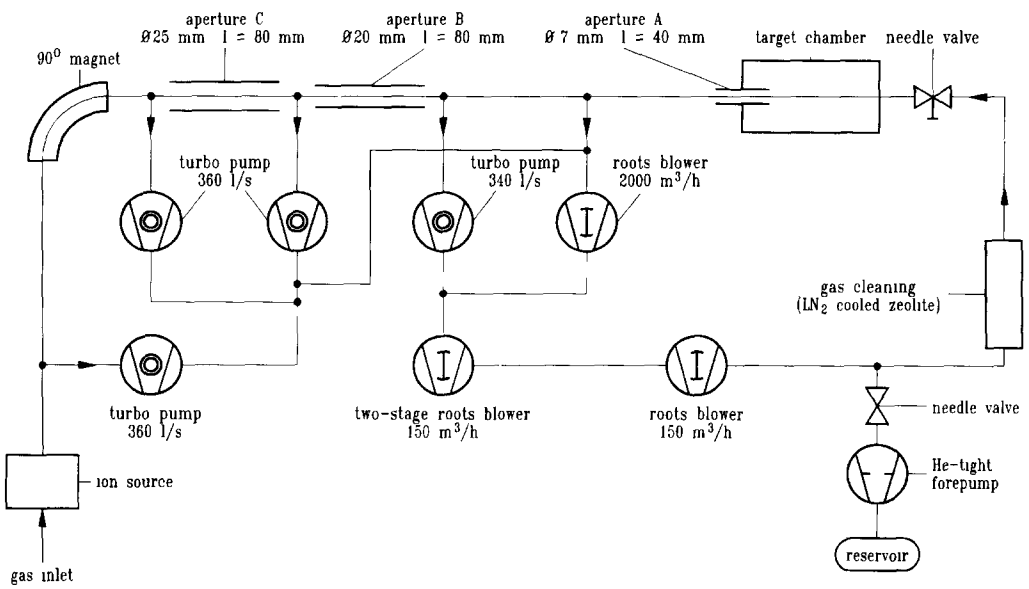

Fig. 3. Schematic diagram of the windowless and recirculating gas target system including the gas flow from the ion source.

250 μA is available. For the windowless gas target system with tight pumping apertures (smallest diameter: 7 mm, Fig. 3 and Section 2.6) a reduction of beam current in the target zone has to be expected. It was found that in the energy range of 30–50 keV a ^{3}He ion beam current of about 500 μA can be focused into the relevant target area, a significant improvement compared to previous work [13] (factor $\simeq$ 1.5 at 50 keV and factor $\simeq$ 3 at 30 keV).

2.6. Windowless gas target system

For the studies of the ^{3}He(^{3}He, 2p)^{4}He reaction a windowless (differentially pumped) and recirculating gas target system [25] of three pumping stages was constructed, consisting of roots blowers and turbo pumps (all from LEYBOLD) with pumping speeds given in Fig. 3. The beam enters the target chamber through three watercooled apertures (A to C) of high gas flow impedance (diameters and lengths are given in Fig. 3) and is stopped in a beam calorimeter. The gas pressure in the target chamber was measured with a Baratron capacitance manometer (model 127, MKS) to an accuracy of better than 1%. This measurement is absolute and independent of the type of gas used. The pressure at several other locations in the gas target system was determined by thermocouple, Penning, and ionization manometers. For ^{3}He gas (99.9% enriched in ^{3}He) of $p = 0.50$ mbar pressure in the target chamber, the three-stage pumping system reduced the pressure to 1×10^{-3}, 1×10^{-4}, and 1×10^{-5} mbar in the regions between the apertures A and B, B and C, and near the analysing magnet, respectively. The gas composition in the target chamber was monitored with a mass spectrometer (model 600A-PPT, MKS). The ^{3}He gas from the three-stage pumping system as well as from the turbo pump at the ion source (base pressure here: 2×10^{-5} mbar) was compressed by two roots blowers and recirculated continuously into the target chamber (Fig. 3). The recirculated gas was cleaned efficiently using a zeolite adsorption trap cooled to liquid nitrogen temperature. The pressure in the target chamber was kept at a constant value using a needle valve (model 248A, MKS) in combination with an electronic regulation unit. Since the (non-recirculated) ^{3}He gas flow from the ion source would increase steadily the gas pressure in the gas target system, a virtual leak was created using a regulated needle valve, a He-tight pump/compressor, and a storage reservoir/buffer (Fig. 3); thus, the amount of ^{3}He gas in the target system could be kept at a constant level.

As noted above, the main pressure drop occurs across the entrance aperture A of the target chamber. It was shown that in the extended gas target chamber the pressure in the observation region of the detectors is essentially unmodified by the gas flow through the entrance aperture A, and the geometrically extended target zone is characterized by a nearly static pressure. However, in determining the gas temperature one must take into account beam-heating effects in the gas, which may raise the local temperature along the beam path. The influence of intense ion beams on the densities of quasi-static gas targets has been studied [26] and found to depend on the beam diameter, the energy loss per unit length, and the ion beam current, i.e., on the dissipated power in the gas. In the present case, the effects on the gas density are less than 0.5% for the maximum 0.50 mbar ^{3}He target pressure and the 500 μA maximum beam current.

2.7. Beam calorimeter

The beam current in the target area was determined to an accuracy of 3% using a beam calorimeter: the beam is stopped in the calorimeter, where the kinetic energy E_{lab} of the projectiles is converted into heat which is measured by the calorimeter. The total integrated beam power $L(t)$ at the calorimeter over a time period t yields the total number of incident projectiles $N(t)$, $N(t) = L(t)/E_{\mathrm{lab}}$. This method ignores the charge state of the incident ions and, when combined with an accurate energy determination (including the energy loss in the target gas), it gives an accurate determination of the number of incident particles in a given run. The problem of heat losses, e.g. via conduction and convection transport mechanisms, has been minimized in the design of a constant temperature gradient [27]. The beam calorimeter (maximum beam power: 25 W) was placed at such a distance from the target area that angle straggling of the incident ion beam in the gas results in a beam profile smaller than the 200 mm^2 active area of the calorimeter.

2.8. Detector setup

One of the most severe problems in previous investigations of the ^{3}He(^{3}He, 2p)^{4}He reaction [13] ($Q = 12.86$ MeV) was the observed yield from the background reaction d(^{3}H, p)^{4}He or ^{3}He(d, p)^{4}He ($Q = 18.35$ MeV) due to a deuterium contamination of order 10^{-7} in the ^{3}He target gas or in the ^{3}He ion beam (as HD$^+$ molecule), which dominated the singles spectra at low energies (due to the lower Coulomb barrier of d + ^{3}He compared with ^{3}He + ^{3}He). To solve this problem [13], two pairs of Si detectors (active area: 450 mm^2, thickness: 500 μm) were placed at opposite sides of the beam axis at a distance of 1 cm from the beam axis. Ni and Al foils of ^{3}He and ^{4}He stopping thickness were placed in front of the detectors. By the requirement of proton–proton coincidences between each detector pair, a unique signature of the ^{3}He(^{3}He, 2p)^{4}He reaction was obtained in the coincidence spectra. The price for this unique signature was a reduction in detection efficiency, by at least an order of magnitude compared to analysis via singles spectra.

In the present approach Monte Carlo calculations [21] have been carried out initially to find the optimum detection setup for realistic experimental conditions (Section 3).

This setup was found in four ΔE–E telescopes placed (in a rectangular target chamber) around the beam axis (Fig. 4) at a distance of 2.5 and 3.5 cm from the beam axis. Each telescope consists of transmission surface barrier detectors with a 0.25 μm thick Al layer deposited on both sides of the detectors (special production by Micron). The ΔE and E detectors both have an active (square) area of 2500 mm^2; the ΔE detector (105 keV energy resolution at $E_\alpha = 5.5$ MeV) has a thickness of 140 μm and the E detector (55 keV energy resolution at $E_\alpha = 5.5$ MeV) has a thickness of 1000 μm (maximum available thickness; the desirable thickness was 1400 μm to stop the 14.7 MeV protons from ^{3}He(d, p)^{4}He). A mylar foil and an Al foil (each of 1.5 μm thickness) are placed in front of each telescope. They stop the intense elastic scattering yields and shield the detectors from beam-induced light and heat (degrading otherwise continuously the signal-to-noise ratio of the detectors). To minimize further the beam-induced heating of the detectors over long running periods, the telescope detectors are cooled using Peltier elements. Finally, to protect the telescopes from beam-induced secondary electrons, Helmholtz coils (producing a magnetic field of up to 15 mT in the detector region parallel to the beam axis) are placed at the beam-entrance and beam-exit side of the target chamber.

The ^{4}He ejectiles from both reactions (^{3}He(^{3}He, 2p)^{4}He: $E_\alpha \simeq 0$ to 4.3 MeV; ^{3}He(d, p)^{4}He: $E_\alpha \simeq 3.7$ MeV) are stopped completely in the ΔE detectors, while the ejected protons from both reactions (^{3}He + ^{3}He: $E_p \simeq 0$ to 10.7 MeV; ^{3}He + d: $E_p \simeq 14.7$ MeV) leave signals in both the ΔE and E detectors of a given telescope. The coincidence requirement between the proton signals, created in the ΔE and E detectors of a telescope, leads to a unique signature of events arising from each reaction (Section 3.3). It is important to point out, that the coincidence requirement also significantly minimized events due to the intrinsic radioactivity of the detectors themselves and of materials surrounding the detectors.

2.9. Electronics and data acquisition system

Standard NIM electronics were used in connection with the four telescopes. The signals were handled and stored

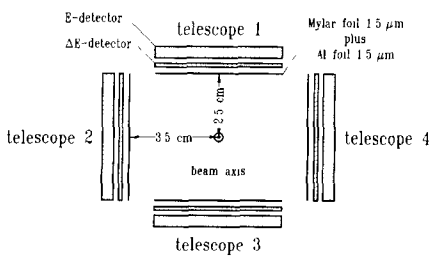

Fig. 4. Setup of four ΔE–E telescopes (surface barrier detectors) placed around the beam axis.

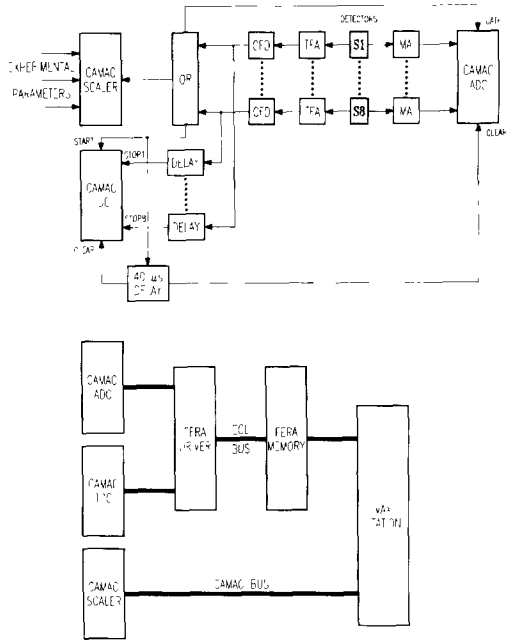

Fig. 5. Schematic diagram of the electronics and the data acquisition system.

using a modular CAMAC multiparameter system based on a VAX computer (Fig. 5), which was developed at the Universita di Genova and can be adapted to other experimental requirements. Briefly, the signals from each surface barrier detector (Si detectors S1 to S8 in Fig. 5) pass through a preamplifier of low noise level (model 2003BT, Canberra) and are amplified by both a main amplifier (MA, model 571, Ortec) and a timing filter amplifier (TFA, model 474, Ortec). The signals from the MA are led to a CAMAC analog-digital-converter (ADC) system (8 ADC, model 4418/v, Silena) and the signals from the TFA are led to a system of constant fraction discriminators (CFD, model CF8000, Ortec), where a threshold above the noise level of the detectors is set. The logic output of the CFD is fed into an OR box (model CO8000, Ortec) delivering a gate signal for the CAMAC ADCs as well as a start signal for a time spectrum via a CAMAC time-digital-converter (TDC) system (8 TDC, model 4418/t, Silena). The stop signal of the TDC is provided also by the CFD with an appropriate delay time. After a delay time of 1 μs, the OR box delivers a "clear" signal to both the CAMAC ADC and CAMAC TDC. Note that the system considers signals as coincident, if they arrive within a time window of 1 μs. This 1 μs time window can be reduced further in play-back data analyses using the TDC spectra. The signals from the ADC and TDC systems are delivered via an ECL bus to a FERA driver (model 4301, LeCroy) and from there to a FERA memory/buffer (model 4302, LeCroy). Via a CAMAC bus the data content of the buffer is transferred to a VAX station (4000-60) and stored on

disk in the PAW package format. The system can handle safely a data flux of about 500 events per second. The acquisition system also stores concurrent information on experimental parameters (such as ion beam current, accelerator HV, and gas pressure in the target chamber) via CAMAC scalers.

The system allows on-line data analysis in order to control the experiment during long running times. Controls have also been implemented to stop data acquisition if the ion beam is lost or to reject an event if an error in the data transmission occurred. Since the two protons ejected in the ^{3}He(^{3}He, 2p)^{4}He reaction can trigger concurrently at most two telescopes, events are rejected if more than two telescopes are triggered. In this way, count rate due to electronic (high frequency) noise in the electronics, caused e.g. by occasional discharges of the accelerator HV, is significantly minimized. Furthermore, rare events due to cosmic ray showers triggering more than two telescopes are also excluded in this way.

2.10. The underground LUNA laboratory at LNGS

The 50 kV accelerator facility has been tested over a period of three months at the DTL in Bochum and moved in late 1993 to LNGS, where it is installed at the underground LUNA laboratory built at node A. The LUNA laboratory consists of an experimental room and a control room (Fig. 6) and is equipped with the necessary infrastructure such as electric power, uninterruptable power supplies, water cooling, liquid nitrogen tank, crane, air conditioning, and computer connections to places outside the laboratory.

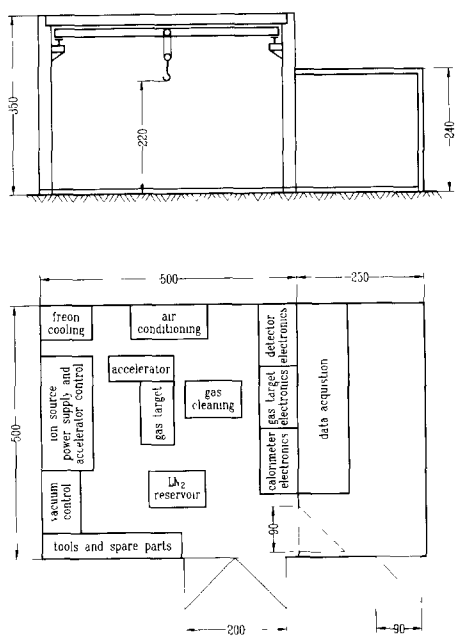

Fig. 6. Diagram of the underground LUNA laboratory at LNGS (the quoted lengths are in cm units).

3. Experimental tests and simulations

In order to optimize the detection setup and to understand the resulting spectra for quantitative analyses, a Monte Carlo program was written to simulate the experimental setup. The program takes into account aspects such as:

- the geometry of the detectors or telescopes, their intrinsic energy resolution, their dead layers, their thickness (e.g. incomplete stopping), and their noise level;
- the energy loss and energy straggling of the projectiles in the target (gas, gas mixture, or solid target, where applicable) and in foils in front of the detectors, using the available compilations [28] and reviews [29];
- kinematic effects on the energies of the ejectiles in the case of a geometrically extended gas target zone as well as thermal translational Doppler broadening;
- yield dependence of the ejectiles on the total and differential cross section over the extended gas target zone.

The program produces energy and time spectra of the ejectiles as well as absolute yields, which can be compared directly with data. From these simulations it was found that a detection system consisting of four telescopes placed around the beam axis was the optimum solution for studies of the ^{3}He(^{3}He, 2p)^{4}He reaction (Section 2.8). Tests using this reaction as well as the d + d and d + ^{3}He induced fusion reactions are described in what follows.

3.1. Solid target setup: singles spectra of d + d fusion reactions

The first test consisted in the measurement of singles spectra of the d(d, n)^{3}He and d(d, p)t fusion reactions at E_{lab}(d) = 10 keV using a deuterium implanted solid target and a circular Si detector (Canberra PIPS, active area: 600 mm^2, thickness: 100 μm, energy resolution: 25 keV at E_α = 5.5 MeV, 1.8 μm thick mylar foil in front of the detector) placed at 130° to the beam axis and at a distance of 5.1 cm from the target. A sample spectrum is shown in Fig. 7 together with the simulated spectrum: good overall agreement is noted in the shape and relative yields of the peaks.

3.2. Gas target setup: studies of d(^{3}He, p)^{4}He

The second test consisted in the measurement of spectra for the reaction d(^{3}He, p)^{4}He in the setup of Fig. 1 at E_{lab}(^{3}He) = 70 keV (here the beam was provided by the 450 kV DTL accelerator) with $p(D_2)$ = 0.05 to 0.10 mbar in the target chamber. This reaction was chosen since it represents an important contaminant reaction in the ^{3}He(^{3}He, 2p)^{4}He studies (Section 2.8). Observed and sim-

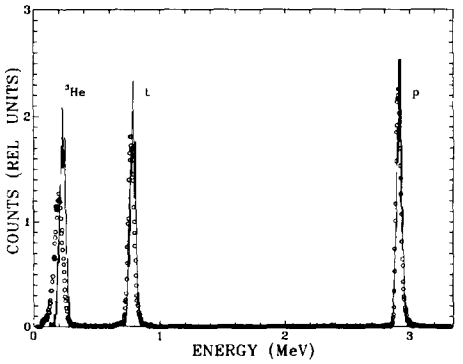

Fig. 7. Sample spectrum of the d(d, n)^{3}He and d(d, p)t reactions as obtained with a solid target at $E_{lab}(d) = 10$ keV. The simulated spectrum is illustrated by the solid curves.

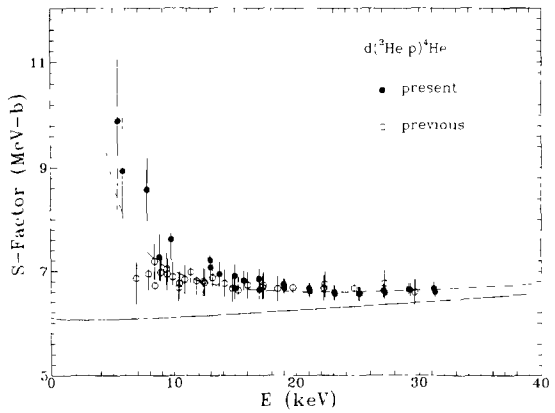

Fig. 9. $S(E)$ factor data from previous [15] and present work for the d(^{3}He, p)^{4}He reaction. The solid curve represents the case for bare nuclides and the dashed curve gives the enhancement due to the effects of electron screening (for details, see text).

ulated spectra for one of the four telescopes (Fig. 4) are illustrated in Fig. 8. The spectra in Fig. 8a display the results for the 140 μm thick ΔE detector, where the low-energy peak represents events of the proton ejectiles (their energy loss) and the broad peak at higher energies the events of the ^{4}He ejectiles, which are fully stopped in the detector. This identification was supported from ΔE spectra obtained in coincidence with the 1000 μm thick E detector in the telescope arrangement (here only the low-energy proton peak was visible). The results for the 1000 μm E detector in the telescope arrangement are shown in Fig. 8b: here only events from the ejected protons are visible, which has been confirmed by spectra obtained in coincidence with the ΔE detector. The broad structure arises from incomplete stopping of protons incident near 90° in the detector, while the peaks at 14.3 and 15.1 MeV arise from kinematic effects in combination with protons incident at the angle range 150°–180° and 0°–44° in the detector, where they are fully stopped. Monte Carlo calculations are in good agreement with these estimates (results of calculations: 148°–180° and 0°–49°). Good agreement is noted between the observed and simulated shape of the spectra.

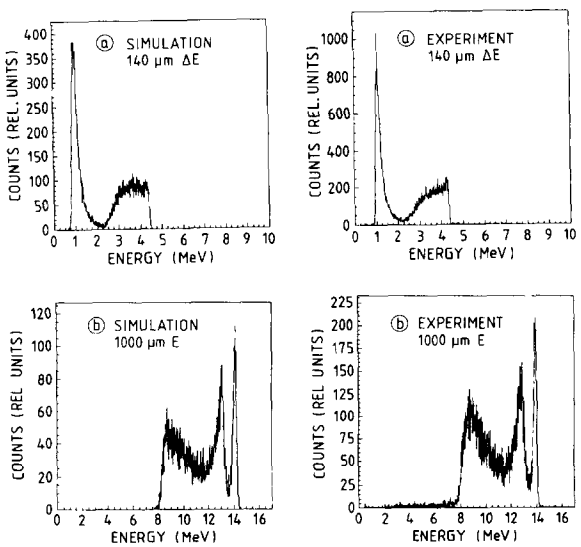

Fig. 8. Observed and simulated spectra of the ^{3}He(d, p)^{4}He reaction at $E_{lab}(^3He) = 70$ keV as obtained with a 140 μm thick ΔE detector and a 1000 μm thick E detector in the telescope arrangement shown in Fig. 4.

As a third test, an excitation function has been obtained in the energy range $E = 5.4$ to 31.3 keV. The resulting absolute $S(E)$ values, deduced with the absolute efficiencies given by the Monte Carlo program, are about 10% higher than the values reported by Engstler et al. [15] and Krauss et al. [30] in the overlapping energy region. In a recent survey [31] the available data of this reaction over a wide energy range have been parametrized by a polynomial function, which is illustrated in Fig. 9 by a solid curve representing at these energies the case of bare nuclides, i.e. the curve does not include at these low energies the effects of electron screening. To arrive at a consistent picture, we have normalised the present data and those of Ref. [15], including the effects of electron screening, to this curve; the individual normalizations in absolute scales amounted to a factor of 0.90 (present data) and 1.004 [15]. The results are shown in Fig. 9, where the dashed curve represents the enhancement due to electron screening with a screening potential of $U_e = 123 \pm 9$ eV. Due to time limitations, the lowest data points were obtained over a running time of only 22 hours with an un-optimized ion beam current. In spite of these restrictions the results demonstrate the potential of the LUNA accelerator facility to carry cross section measurements to energies far below those of previous work.

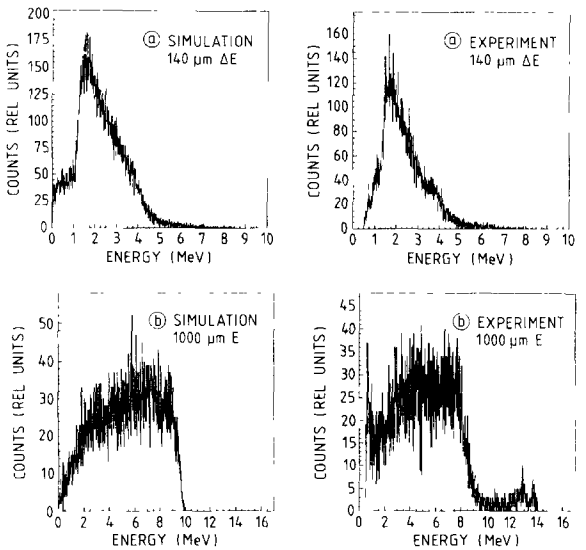

Fig. 10. Observed and simulated spectra of the ^{3}He(^{3}He,2p)^{4}He reaction at $E_{lab}(^3He) = 150$ keV as obtained with a 140 μm thick ΔE detector and a 1000 μm thick E detector in the telescope arrangement shown in Fig. 4.

3.3. Gas target setup: studies of ^{3}He(^{3}He, 2p)^{4}He

As a further test, spectra of the ^{3}He(^{3}He, 2p)^{4}He reaction were obtained in the setup of Fig. 1 at $E_{lab}(^3He) = 150$ keV and $p(^3He) = 0.10$ mbar. The resulting singles spectra for the ΔE and E detectors are displayed in Fig. 10 together with the simulations: good agreement is noted. The simulated spectrum ignored the presence of deuterium nuclides in the system, while the high-energy part of the observed spectrum of the E detector exhibits clearly their presence. The corresponding ΔE–E diagrams (telescope) are shown in Fig. 11, where the simulated spectrum assumed a gas mixture of $D/^3He = 4 \times 10^{-6}$ in the system. Again good agreement is noted in the relative distribution

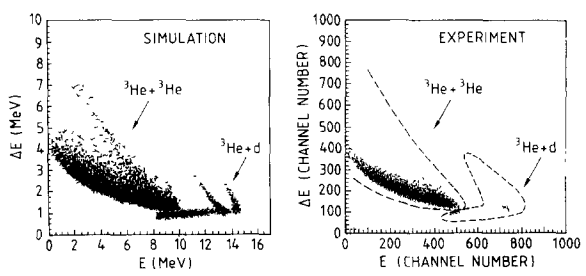

Fig. 11. Observed and simulated ΔE–E diagrams of the telescope in the setup of Figs. 1 and 4 for the ^{3}He(^{3}He,2p)^{4}He and d(^{3}He, p)^{4}He reactions at $E_{lab}(^3He) = 150$ keV. The simulated spectrum assumed a gas mixture of $D/^3He = 4 \times 10^{-6}$ in the target area. The dashed curves in the observed diagram indicate the selected regions for data analyses.

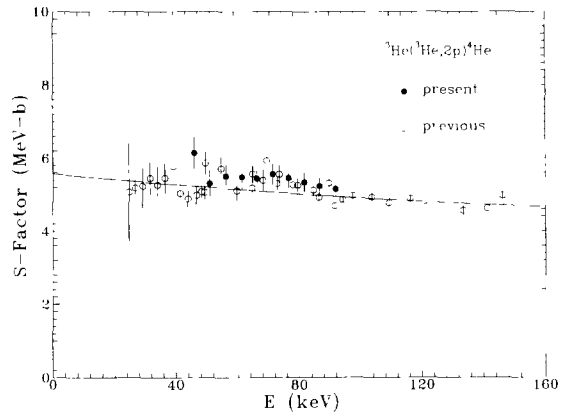

Fig. 12. $S(E)$ factor data from previous [13] and present work for the ^{3}He(^{3}He,2p)^{4}He reaction. The solid curve represents the polynomial fit to the previous data with $S(0) = 5.5$ MeV b.

of events. The results show also that the events from the ^{3}He(^{3}He, 2p)^{4}He reaction can be clearly separated from those of the contaminant reaction ^{3}He(^{3}He, 2p)^{4}He, even in the "touching" region near $\Delta E \simeq 1$ MeV and $E \simeq 9$ MeV. It was found that the touching region overlaps increasingly if the noise level (i.e. the energy resolution) of the detectors deteriorates with time. Thus, cooling of the telescopes (to about 0°C) represents a necessary requirement.

As a final test, an excitation function was obtained over the energy region $E = 46$ to 92 keV. The results (Fig. 12) are in good agreement with previous work [13] both in the energy dependence as well as in the absolute scale. In spite of similar restrictions as quoted above (Section 3.2), the results demonstrate the feasibility of the LUNA accelerator facility for the main goal of this pilot project.

Background measurements at the DTL in Bochum showed that cosmic rays produce events within the ΔE–E region of the ^{3}He(^{3}He, 2p)^{4}He reaction (Fig. 11) in the amount of 3.5×10^{-4} events/s, while in the underground LUNA laboratory at LNGS this rate was observed [21] to be reduced by at least a factor 200.

3.4. Summary

The reduction in cosmic ray background together with a higher beam current (factor 3 at 30 keV) and a higher detection efficiency (factor 20) led to an improvement in experimental sensitivity by at least a factor 12000 compared to previous work [13]. Thus, it appears possible to study the ^{3}He(^{3}He, 2p)^{4}He reaction over the entire thermal energy range in the sun ($E_0 = 16$ to 27 keV), requiring however running times of several months. The long term stability of the LUNA accelerator facility has been verified, at least over a three month test period at Bochum.

Acknowledgements

The authors thank Prof. P. Monacelli for the hospitality at LNGS and the administration and technical staff at LNGS for their support. The technical help of G. Krüger, J. Wöhlert, the staff of the mechanical and electronic workshops at Bochum, and the staff of the electronic workshop at Münster is highly appreciated.

References

[1] W.A. Fowler, Rev. Mod. Phys. 56 (1984) 149.
[2] C. Rolfs and W.S. Rodney, Cauldrons in the Cosmos (University of Chicago Press, 1988).
[3] J.N. Bahcall, W.F. Huebner, S.H. Lubow, P.D. Parker and R.K. Ulrich, Rev. Mod. Phys. 54 (1982) 767.
[4] R. Davis and A.N. Cox, Solar neutrino experiments, Solar Interior and Atmosphere, eds. A.N. Cox, W.C. Livingston and M.S. Matthews (University of Arizona Press, 1991).
[5] P. Parker and C. Rolfs, Nuclear energy generation in the solar interior, Solar Interior and Atmosphere, eds. A.N. Cox, W.C. Livingston and M.S. Matthews (University of Arizona Press, 1991).
[6] N.M. Wang, V.M. Novatskii, G.M. Osetinskii, N.K. Chien and I.A. Chepurchenko, Sov. J. Nucl. Phys. 3 (1966) 777.
[7] A.D. Bacher and T.A. Tombrello, quoted by T.A. Tombrello, Nuclear research with Low-Energy Accelerators, eds. J.B. Marion and D.M. van Patter (Academic Press, 1967) p. 195.
[8] M.R. Dwarakanath and H. Winkler, Phys. Rev. C 4 (1971) 1532.
[9] W.A. Fowler, Nature 238 (1972) 24.
[10] V.N. Fetisov and Y.S. Kopysov, Phys. Lett. B 40 (1972) 602; Nucl. Phys. A 239 (1975) 511.
[11] A.B. McDonald, T.K. Alexander, J.E. Beene and H.B. Mak, Nucl. Phys. A 288 (1977) 529.
[12] M.R. Dwarakanath, Phys. Rev. C 9 (1974) 805.
[13] A. Krauss, H.W. Becker, H.P. Trautvetter and C. Rolfs, Nucl. Phys. A 467 (1987) 273.
[14] H.J. Assenbaum, K. Langanke and C. Rolfs, Z. Phys. A 327 (1987) 461.
[15] S. Engstler, A. Krauss, K. Neldner, C. Rolfs, U. Schröder and K. Langanke, Phys. Lett. B 202 (1988) 179.
[16] C. Angulo, S. Engstler, G. Raimann, C. Rolfs, W.H. Schulte and E. Somorjai, Z. Phys. A 345 (1993) 231.
[17] E. Bellotti, Nucl. Instr. and Meth. A 264 (1988) 1.
[18] MACRO Collaboration, Phys. Lett. B 249 (1990) 149.
[19] U. Greife, Thesis, Ruhr-Universität Bochum (1994).
[20] F. Gorris, Diplomarbeit, Ruhr-Universität Bochum (1994).
[21] A. Lanza, Tesi di Laurea in Fisica, Universita di Genova (1994).
[22] R.G. Wilson and G.R. Brewer, Ion Beams (Wiley, 1973).
[23] R.E. Brown and N. Jarmie, Phys. Rev. C 41 (1990) 1391.
[24] K. Neldner, H.W. Becker, S. Engstler, M. Köster, C. Rolfs, U. Schröder, W.H. Schulte, H.P. Trautvetter and K. Brand, Nucl. Instr. and Meth. A 274 (1989) 419.
[25] C. Rolfs, J. Görres, K.U. Kettner, H. Lorenz-Wirzba, P. Schmalbrock, H.P. Trautvetter and W. Verhoeven, Nucl. Instr. and Meth. 157 (1978) 19.
[26] J. Görres, K.U. Kettner, H Kräwinkel and C. Rolfs, Nucl. Instr. and Meth. 177 (1980) 295.
[27] A. Vlieks, M. Hilgemeier and C. Rolfs, Nucl. Instr. and Meth. 213 (1983) 291.
[28] J.F. Ziegler, Program TRIM-91, The Transport of Ions in Matter (IBM Research, New York, 1991).
[29] F. Besenbacher, J.U. Anderson and E. Bonderup, Nucl. Instr. and Meth. 168 (1980) 1.
[30] A. Krauss, H.W. Becker, H.P. Trautvetter, C. Rolfs and K. Brand, Nucl. Phys. A 465 (1987) 150.
[31] G.S. Chulik, Y.E. Kim and R.A. Rice, Nucl. Phys. A 551 (1993) 255.